Physica B 678 (2024) 415780

Contents lists available at ScienceDirect

Physica B: Condensed Matter

journal homepage: www.elsevier.com/locate/physb

Elastic, mechanical and thermodynamic properties of technetium-based perovskites $XTcO_3$ (X = K, Rb) compounds

Toufik Nouri [a], Friha Khelfaoui [a], Kadda Amara [a], Abdelmadjid Bouhemadou [b], Fadila Belkharroubi [c], Y. Al-Douri [d,e,*]

[a] Laboratory of Physicochemical Studies, University of Saida-Dr. Moulay Tahar, Saida, 20000, Algeria
[b] Laboratory for Developing New Materials and Their Characterizations, Ferhat Abbas University - Setif 1, 19000, Setif, Algeria
[c] Laboratory of Analysis and Aplication of Radiations (LAAR), Faculty of Physics, University of Science and Technology of Oran Mohamed Boudiaf (USTO-MB), 1505 El Menouar, 31000, Oran, Algeria
[d] Department of Mechanical Engineering, Faculty of Engineering, Piri Reis University, Eflatun Sk. No:8, 34940, Tuzla, Istanbul, Turkey
[e] Nanotechnology and Catalysis Research Centre, University of Malaya, 50603, Kuala Lumpur, Malaysia

ARTICLE INFO

Keywords:
Perovskite
Mechanical
Elastic
Thermodynamic
Electronic

ABSTRACT

ab-initio calculations are employed to determine the structural, mechanical, elastic, electronic and thermodynamic properties of perovskite oxides $XTcO_3$ (X = K, Rb). From the computed structural properties, $KTcO_3$ and $RbTcO_3$ are found to be stable with equilibrium lattice constants; 7.3943 Bohr and 7.4909 Bohr, respectively. From electronic structure results, a metallic character is remarked for both compounds. The determined elastic constants (C_{11}, C_{12}, C_{44}) have indicated the mechanical stability of $XTcO_3$ (X = K, Rb) compounds that is confirmed by the phonon spectra. In addition, $KTcO_3$ is found to be isotropic and $KTcO_3$ is nearly isotropic according the anisotropic constant A values. B/G ratio has indicated the brittleness of both compounds. Furthermore, the Helmholtz free energy (F), entropy (S) and heat capacity (C_V) are determined using QHA (Quasi harmonic Approximation). Our computational indicates that $XTcO_3$ (X = K, Rb) compounds can be used as new materials for solid oxide fuel cells and related applications.

1. Introduction

Perovskite materials have received much attention both theoretically and experimentally due to their wide range of properties, such as optoelectronic, electronic, ionic conductivity, piezoelectricity, superconductivity, ferroelectricity and half-metallicity [1–4]. Today, researchers are looking for perovskite materials that are able to boost modern technology that is priority in material science. For example, halide perovskites are proved to have a high performance materials for solar cells applications [5]. They can be metals, insulators, semi-conductors or half-metallic materials based on the electronic behavior [6].

Perovskite oxides ABO_3 have gained particular interest of researchers for the last years and still being studied continuously for their properties including anti-ferromagnetism ($LaMnO_3$) [7], ferroelectricity ($BaTiO_3$) [8], ferro-elasticity ($SrTiO_3$) [9], anti-ferroelectricity (KIO_3) [10], ferromagnetism ($YTiO_3$) [11], half-metal ferromagnets and their importance in modern technology. ABO_3 compounds commonly crystallize in a cubic structure with a space group Pm-3 m, where A cations are located at eight corners, oxygen anions occupy six face centers of cube, and body center is occupied by B cation. Lead-based oxide perovskites like $PbTiO_3$ [12], $PbZrO_3$ [13], $PbMgO_3$ [14], $PbMoO_3$ [15] have been proved to have good ferroelectric and piezoelectric characters, however, lead compounds are not stable under ambient conditions and, therefore, decompose into substances that are harmful and toxic to the environment [16,17]. To limit the negative influence of lead element to the environment, the proposed strategy is to substitute lead element by another substance. Therefore, investigating efficient lead-free perovskites [18] for solar cells and optoelectronic devices is essential. Perovskites with a cubic structure have showed a good contribution to ionic conductors and topological insulators [19].

In looking for potential perovskite materials with specific properties for particular applications, computational tools are extensively used these days to predict the properties of materials. Density Functional Theory (DFT) is one of the most accurate and widely used computationally. DFT has been utilized to investigate the properties of rhenium-based perovskite materials $XReO_3$ (X = Rb, Cs, and Ti) [20], $XReO_3$(X =

* Corresponding author. Department of Mechanical Engineering, Faculty of Engineering, Piri Reis University, Eflatun Sk. No:8, 34940, Tuzla, Istanbul, Turkey.
E-mail address: yaldouri@yahoo.com (Y. Al-Douri).

https://doi.org/10.1016/j.physb.2024.415780
Received 8 January 2024; Accepted 15 February 2024
Available online 15 February 2024

Li, Be) [21], $NaReO_3$ and $KReO_3$ [22]. Motivated potential of oxides perovskites, we have investigated the elastic, mechanical and thermodynamic properties of technetium-based perovskites $XTcO_3$ (X = K, Rb), which are not available in the literature right now.

This work is divided into the following: section 2 presents the computational details. In section 3, the results of structural, electronic, elastic, mechanical, and thermodynamic of $XTcO_3$ (X = K, Rb) perovskites are analyzed. Finally in section 4, conclusions are outlined.

2. Computational details

Quantum ESPRESSO code [23–25], which is based on planewave-pseudopotential method [26] is used to investigate the properties of $XTcO_3$ (X = K, Rb) perovskites. Generalized gradient approximation (GGA) [27] with Perdue-Burke Ernzerh (PBE) [28] is used in *ab-initio* calculations for the exchange and correlation energy, adopting the Projected Augmented Wave (PAW) [29] pseudopotential from (SSSP) library. The kinetic energy cut off for the wave function is set to 50 Ry and charge density is 400 Ry. Thresholds are set to 10^{-9} Ry/Bohr on force and 10^{-10} Ry on total energy. To describe the reciprocal k-space, a dense mesh grid of 10 × 10 × 10 k points in the irreducible Brillouin zone according to Monkhorst Pack scheme. Phonons are computed using density functional perturbation theory (DFPT). Thermo_pw package [30] as integrated in Quantum Espresso package is used to obtain the structural stability for computing the elastic constants. Furthermore, thermodynamic properties are calculated using the quasi-harmonic approximation [31]. The valence electronic configuration of different elements is as follows: K ($5s^1$), Rb ($5s^1$), Tc ($4d^5 5s^2$), and O ($2s^2 2p^4$).

3. Results and discussion

3.1. Structural and electronic properties

The structure of perovskite compounds $XTcO_3$ (X = K, Rb) represents a cubic structure with space group Pm-3m (N^o 221), where atoms are located as X (0,0,0), Tc (0.5,0.5,0.5) and O (0,0.5,0.5), (0.5,0.5,0) (0.5,0,0.5) sites. To explore the structural stability of $XTcO_3$ (X = K, Rb), we have calculated total energy with respect to volume, then the equation of states (EOS) proposed by Murnaghan [32] is used to obtain the fitted curve of energy versus volume as shown in Fig. 1. So, the equilibrium lattice constants values; 7.3943 Bohr and 7.4909 Bohr for $KTcO_3$ and $RbTcO_3$, respectively are gotten. The calculated ground state structural results at equilibrium are presented in Table 1 such as bulk modulus (B_0) and pressure derivative of bulk modulus (B′).

To further verify the thermodynamic stability, we have computed the formation energy [33] defined as $E_{for} = E_{(K,Rb)TcO_3}{}^{tot} - (E_{Tc}^{bulk} + E_{K.Rb}^{bulk} + 3E_{O_2}/2)$ where $E_{(K,Rb)TcO_4}{}^{tot}$ is total energies for $KTcO_3$ and $KTcO_3$, respectively, E_{Tc}^{bulk} , $E_{K.Rb}^{bulk}$ represent bulk energies of Tc and K/Rb, respectively. E_{O_2} is energy of O_2 molecule. The computed formation energies for $XTcO_3$ (X = K, Rb) compounds are given in Table 1. The negative values indicate that both materials are thermodynamically stable and therefore can be synthesized experimentally.

The phonon spectra are computed in the first Brillouin zone with Quantum Espresso by using DFPT [34], the computed phonon results are plotted in Fig. 2. Both figures illustrate the dynamical stability of $XTcO_3$ (X = K, Rb) compounds.

Band structures results of $XTcO_3$ (X = K, Rb) materials have been calculated within GGA and drawn along the high symmetry Brillouin zone as presented in Fig. 3 for $XTcO_3$ (X = K, Rb), respectively. It is clear that these compounds present a metallic nature because few bands cross the Fermi level and therefore, there is no gap can be observed.

To understand more about the electronic behavior, we have calculated and plotted total and partial density of states for both compounds as depicted in Fig. 4. The DOS results are nearly the same for both compounds, confirming their metallic character. This behavior is found due to contribution of Tc and O atoms at Fermi-level in both compounds, originating from Tc-d and O-p states. K and Rb states are primarily found in the valance band. Therefore, from Fig. 4, we conclude that all the studied materials present a metallic character, have attributed to presence of Tc-d and O-p states at Fermi level in both compounds.

Table 1
Computed equilibrium lattice parameter a_0 in (Bohr), bulk modulus in (GPa) derivative of bulk modulus with respect to pressure *B'* and formation energy in (Ry) of $XTcO_3$ (X = K, Rb) Compounds.

	a_0	B	B'	E_{for}
$KTcO_3$	7.3943	1836.539	4.731	−0.172
$RbTcO_3$	7.4909	1765.301	4.765	−0.176

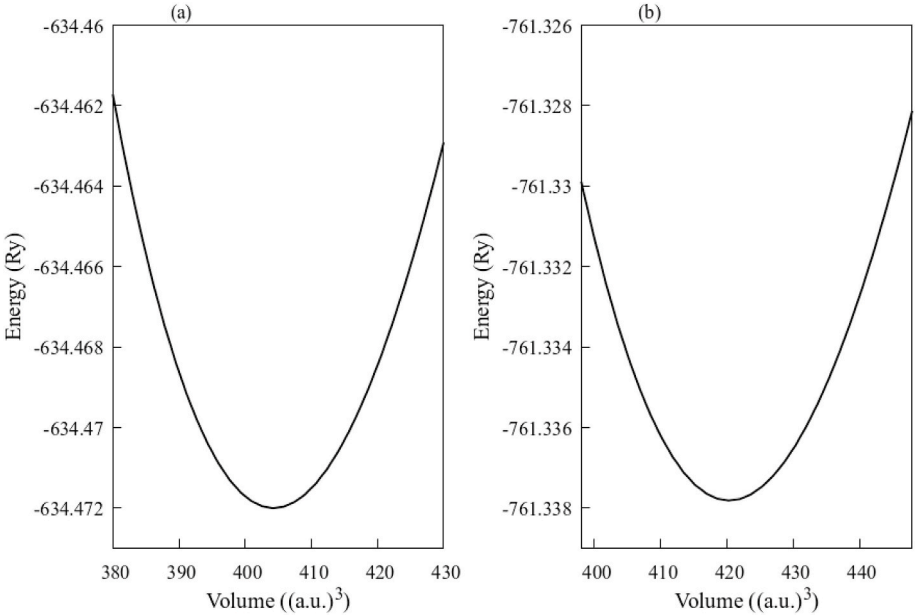

Fig. 1. Energy versus volume optimization curve of (a) $KTcO_3$ and (b) $RbTcO_3$ compounds.

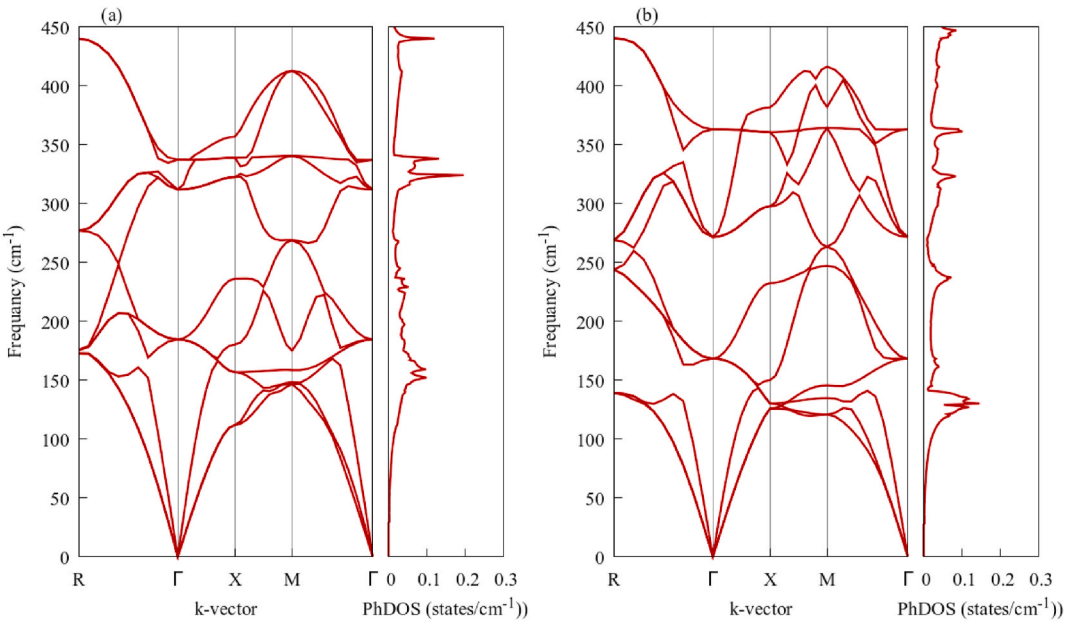

Fig. 2. Phonon dispersion curves of (a)$KTcO_3$ and (b) $RbTcO_3$ compounds.

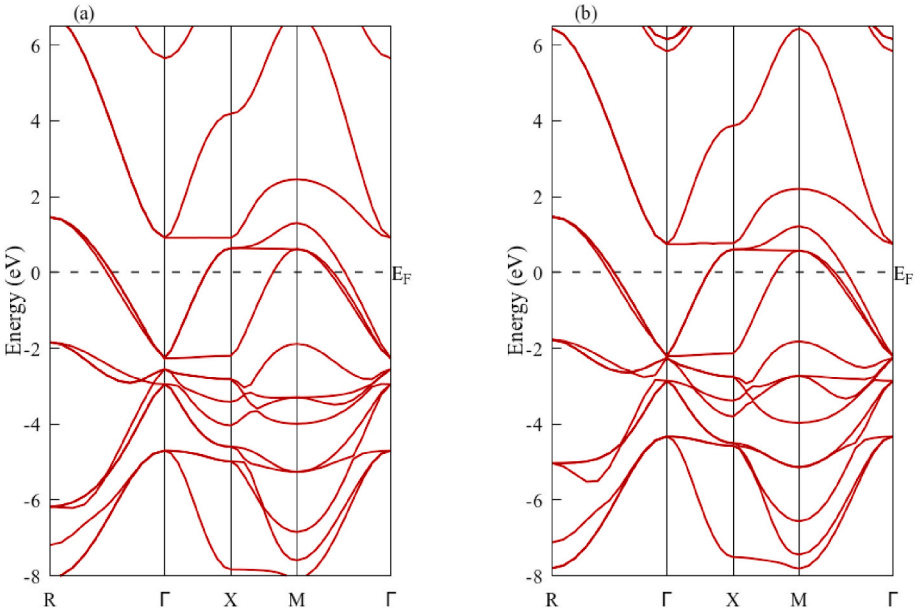

Fig. 3. Electronic band structure (a) $KTcO_3$ and (b) $RbTcO_3$ compounds.

3.2. Elastic and mechanical properties

Calculating the elastic constants of materials is crucial to understand the main features of elastic and mechanical properties by providing important information as far as the mechanical stability, ductility and anisotropy. The obtained values of elastic constants (C_{11}, C_{12}, C_{44}) are computed with Quantum Espresso as presented in Table 2.

The calculated elastic constants for both compounds are found to respect the stability criteria for cubic structure [35,36]: $C_{11} > 0$, $(C_{11}–C_{12}) > 0$, $(C_{11} + 2C_{12}) > 0$, $C_{12} < B < C_{11}$, $C_{44} > 0$. Furthermore, the mechanical parameters like Young's modulus (Y), shear modulus (G), anisotropic factor (A), bulk modulus (B) and Poisson's ratio for both materials are determined from the elastic constants values. From (C_{11}, C_{12}, C_{44}), one obtains Hill's shear modulus (G), determined from the (G_R) Reuss and (G_V) Voigt approximation as follows:

$$G = \frac{G_V + G_R}{2};\ G_V = \frac{C_{11} - C_{12} + 3C_{44}}{5};\ G_R = \frac{5C_{44}(C_{11} - C_{12})}{4C_{44} + 3(C_{11} - C_{12})} \quad (1)$$

Ductility of these materials has been investigated from the ratio (B/G), that is the bulk modulus divided by the shear modulus, the Pugh's criteria states that a material behaves in ductile manner if $B/G > 1.75$, otherwise it is brittle [37,38], B/G are found to be 1.54 and 1.62 for $XTcO_3$ (X = K, Rb), respectively. Thus, from B/G values it is shown that both compounds behave as brittle. In addition, Poisson's ratio is used to learn about the type of bonding that exists in a material [39]. For less than 0.10, the bonding type is covalent, metallic if υ is greater than 0.33 and ionicity υ is included between 0.25 and 0.33. According to our results, the value of Poisson's ratio is quite near to 0.25 for both $KTcO_3$ and $RbTcO_3$; hence, ionic bonding is dominant in both compounds. The Poisson's ratio relation is given by:

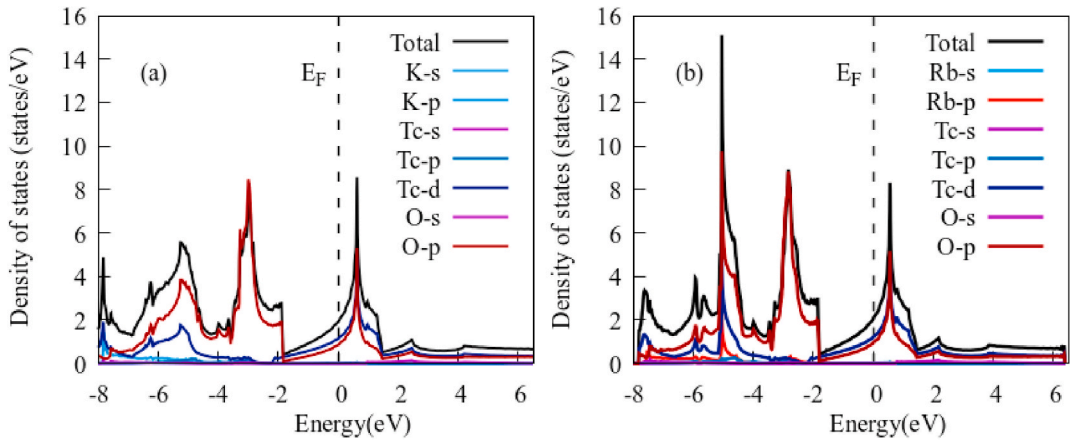

Fig. 4. Total and partial density of states of (a) $KTcO_3$and (b) $RbTcO_3$compounds.

Table 2
Values of elastic constants C_{ij}(GPa), bulk modulus B (GPa), shear modulus G (GPa), Young'smodulus E (GPa), Poisson's ratio (υ), Pugh ratio B/ G ,Shear anisotropy factor (A) Cauchy pressure C_P(GPa),sound velocities in (m/s), Debye temperature θ_D (K) and melting temperature T_m(K) of $KTcO_3$ and $RbTcO_3$ compounds.

Material Property	$KTcO_3$	$RbTcO_3$
C_{11}	393.764	318.332
C_{12}	78.358	105.373
C_{44}	99.059	111.407
B	183.494	176.604
G	119.437	109.334
E	294.4	271.893
υ	0.232	0.2434
$B/\ G$	1.54	1.62
C_P	315.406	212.959
A	0.628	1.046
v_l	8173.549	7228.012
v_t	4824.979	4209.308
v_m	5318.319	4668.940
$\theta_D(K)$	691.989	599.635
$T_m(K)$	2860.5 ±300K	2434.66 ±300K

$$\upsilon = \frac{9BG}{3B+G} \tag{2}$$

The computed values of E are found to be 294.4 (271.893) GPa for $KTcO_3$ and $RbTcO_3$, respectively. Thus, the values of E indicate that $KTcO_3$ is stiffer compared to $RbTcO_3$, E is written as:

$$E = \frac{3B-2G}{2(3B+G)} \tag{3}$$

We have also determined the value of Bulk modulus for both materials. Bulk modulus B values are found to be 183.494 GPa and 176.604 GPa, respectively for $KTcO_3$ and $RbTcO_3$, respectively. Both Young's modulus and bulk modulus values indicate that our compounds enough stiffness. Hence, both compounds may be used to construct electrode materials for fuel cells [20].

$$B = \frac{C_{11}+2C_{12}}{3} \tag{4}$$

The anisotropy factor A is used to describe the elastic anisotropy [40], A is calculated using the following equation:

$$A = \frac{2C_{44}}{C_{11}-C_{12}} \tag{5}$$

If A equals one, the material is perfectly isotropic, else the material is anisotropic and A is different from unity [41,42]. Our results show that A for $KTcO_3$ equals to 0.628, while for $RbTcO_3$A equals to 1.046 as presented in Table 2. These values indicate the anisotropic behavior $KTcO_3$ and a nearly isotropic behavior for $RbTcO_3$.

Another useful method for investigating other anisotropic behavior of any compound is the three-dimensional (3D) surfaces visualization of Bulk modulus B, Shear modulus G and. Young modulus E. The mechanical moduli depend on crystallographic directions for a cubic system that are computed using the following expressions [43,44].

$$\frac{1}{B} = (S_{11}+2S_{12})\left(I_1^2+I_2^2+I_3^2\right) \tag{6}$$

$$\frac{1}{E} = S_{11} - 2\left(S_{11}-S_{12}-\frac{1}{2}S_{44}\right)\left(I_1^2I_2^2+I_2^2I_3^2+I_3^2I_1^2\right) \tag{7}$$

$$\frac{1}{G} = S_{44} - 4\left(S_{11}-S_{12}-\frac{1}{2}S_{44}\right)\left(Sin^2\,\theta\,Cos^2\,\theta + 0.125\times Sin^4\,\theta\right)(1-cos\,4\,\varphi) \tag{8}$$

where $I_1 = sin\,\theta\,cos\,\varphi$, $I_2 = sin\,\theta\,sin\,\varphi$ and $I_3 = cos\,\theta$ denote the direction cosines along x-axis, y-axis, and z-axis, respectively and S_{ij} is compliance matrix constants. The values of S_{11}, S_{12} and S_{44} equal to 0.0027192 (0.0037651), −0.0004513 (−0.0009388), 0.00100958 (0.0089761) for $KTcO_3$ ($RbTcO_3$), respectively. The 3D surfaces spherical shapes of Bulk modulus B, Young modulus E and Shear modulus G indicate the material's isotropy, whereas the non-spherical shape indicate its anisotropy. The three-dimensional surfaces with their 2D projections of elastic moduli on different planes [100], [001] and [010], G for $KTcO_3$ and $RbTcO_3$ compounds as illustrated in Figs. 5 and 6, respectively.

The 3D plot of bulk moduli exhibits a perfect spherical shape for both compounds revealing an isotropic character for B. Also, the two-dimensional projections of bulk on (100), (001) and (010) planes show an isotropic character for B. As can be seen from Figs. 5, 6 and 3D surfaces of shear moduli and Young's moduli are not spherical $KTcO_3$, but these surfaces are nearly spherical for $RbTcO_3$. Consequently, $KTcO_3$ has anisotropic character and $RbTcO_3$ has nearly isotropic character. The Cauchy pressure C_p [45] values are positive for both compounds that prove the existence of metallic non-directional bonding in these compounds.

The Debye temperature is an important parameter, which is related to many physical properties, such as thermal expansion, specific heat and melting temperature. One of the methods to estimate Debye temperature θ_D is from elastic constants data, calculated Debye temperature values θ_D are 691.989 K and 599.635 K for $KTcO_3$ and $RbTcO_3$, respectively. So, θ_D is expressed by:

$$\theta_D = \frac{h}{k_B}\left[\frac{3}{4\pi V_s}\right]^{\frac{1}{3}} v_m \tag{9}$$

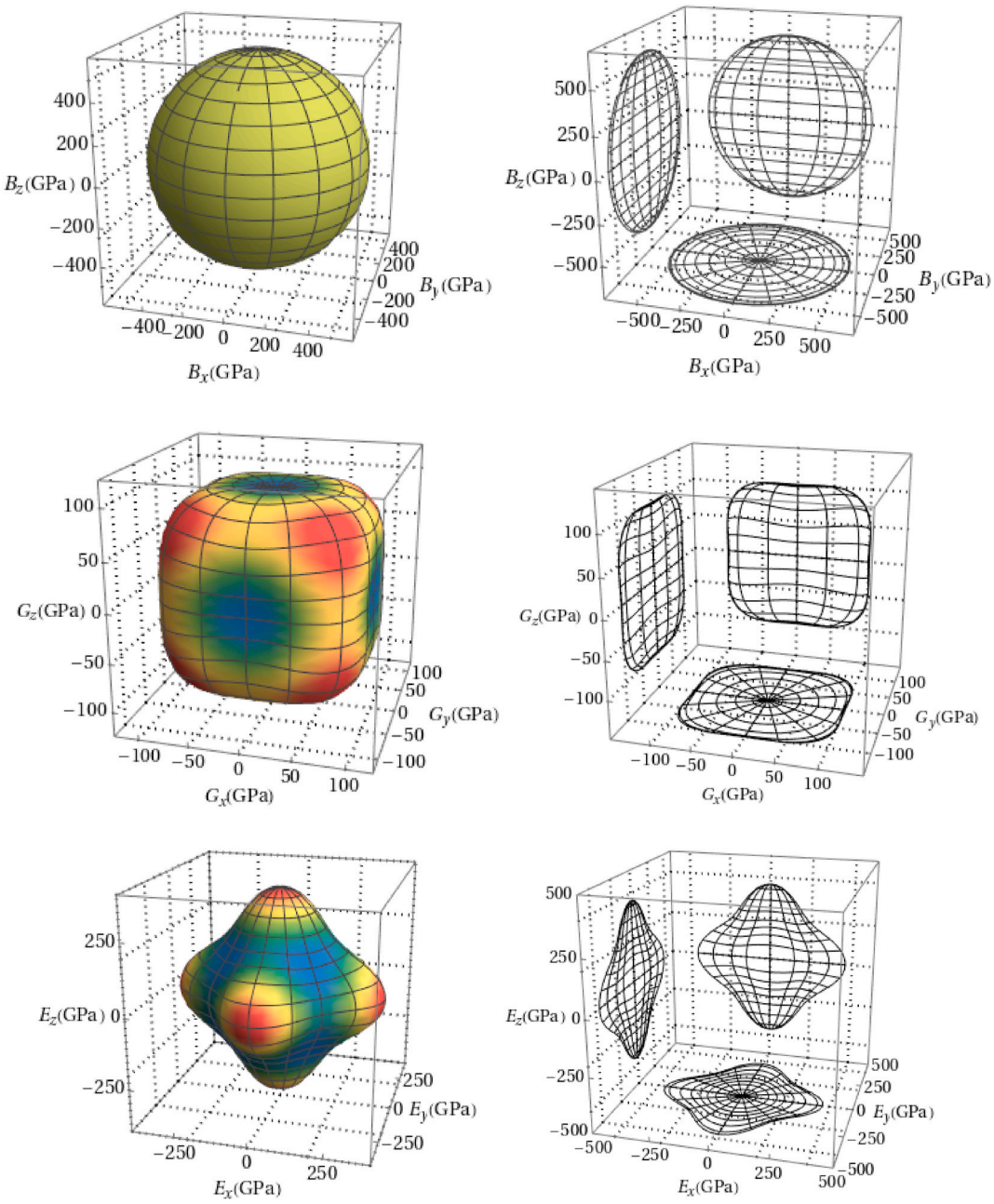

Fig. 5. 3D-directional representation of (a) Bulk modulus B, (b) Young modulus E and Shear (c) modulus G and (d) their projections in different planes (100), (010) and (001) of $KTcO_3$ compound.

where v_m is average wave velocity defined by following relation:

$$v_m = \frac{1}{3}\left[\frac{2}{v_t^3} + \frac{1}{v_l^3}\right]^{\frac{1}{3}} \tag{10}$$

where v_t and v_l are the transverse the longitudinal elastic wave velocities expressed by the following equations:

$$v_t = \left(\frac{G}{\rho}\right)^{\frac{1}{2}}, v_l = \left(\frac{3G+4B}{3\rho}\right)^{\frac{1}{2}} \tag{11}$$

Furthermore, we have computed the melting temperature (T_m) of $XTcO_3$ (X = K, Rb). Using the equation: $T_m(K) = [553(K) + (5.911)C_{11}] \pm 300$. The melting temperature is determined using the elastic constants values and given in Table 2. For both materials, T_m value is sufficiently high.

3.3. Thermodynamic properties

Thermodynamic properties of $XTcO_3$ (X = K, Rb) have been computed using the quasi-harmonic approximation (QHA) model. Heat capacity C_V, Helmholtz free energy F, and entropy S are expressed by the following equations:

$$C_V = \left(\frac{\partial E}{\partial T}\right)_V = \sum_{k,\nu} k_B \left(\frac{\hbar\omega(k,\nu)}{k_B T}\right)^2 \frac{e^{\hbar\omega(k,\nu)/k_B T}}{\left(e^{\hbar\omega(k,\nu)/k_B T} - 1\right)} \tag{12}$$

$$F = -k_B T \ln Z = \varphi + \frac{1}{2}\sum_{k,\nu}\hbar\omega(k,\nu) + k_B T \sum_{k,\nu} \ln\left(1 - e^{-\hbar\omega(k,\nu)/k_B T}\right) \tag{13}$$

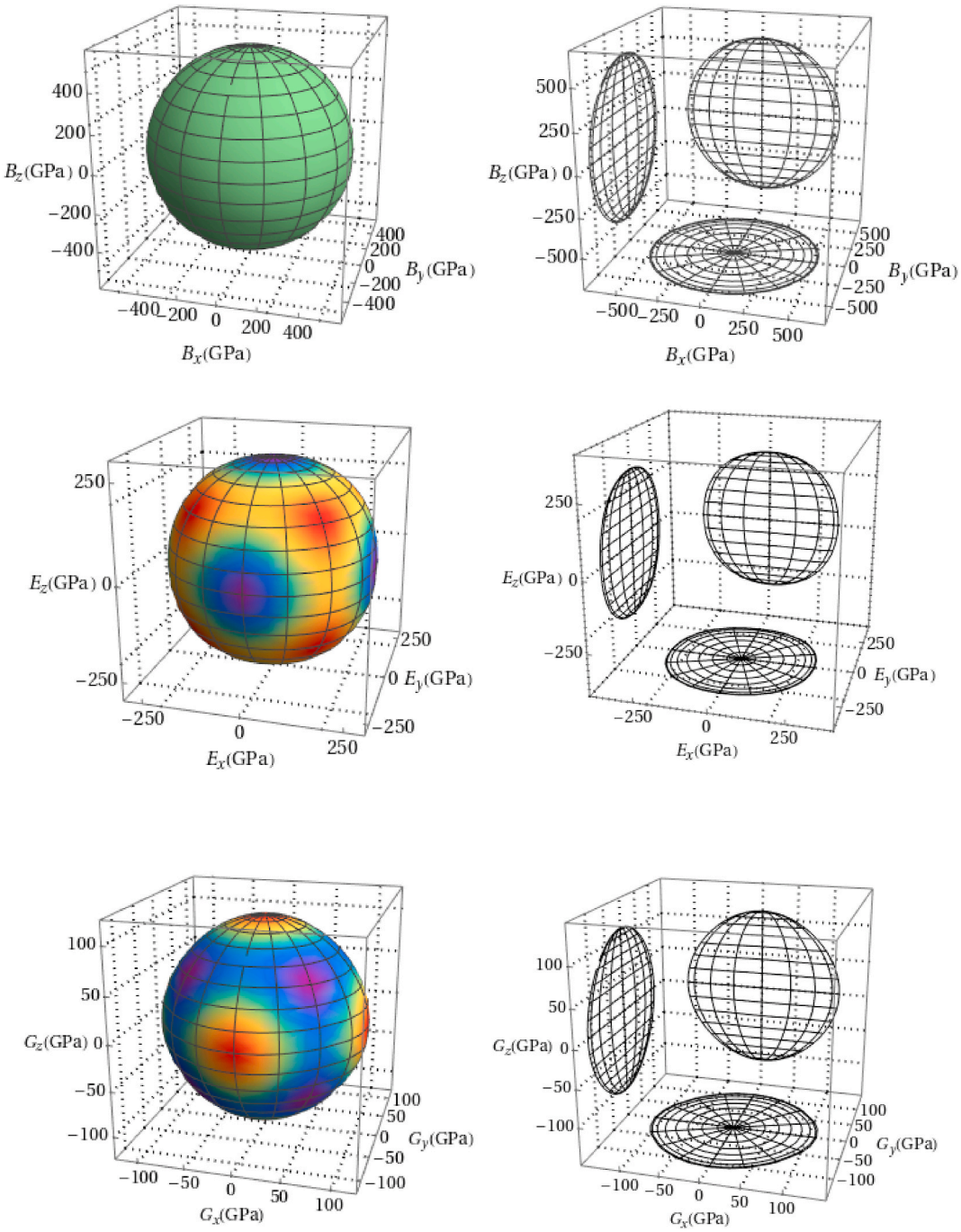

Fig. 6. 3D-directional representation of (a) Bulk modulus B, (b) Young modulus E and Shear (c) modulus G and (d) their projections in different planes (100), (010) and (001) of $RbTcO_3$compound.

$$S = -\frac{\partial F}{\partial T} = \frac{1}{2T}\sum_{k,\nu}\hbar\omega(k,\nu)coth\left(\frac{\hbar\omega(k,\nu)}{2k_BT}\right) - k_B\sum_{k,\nu}\ln\left(2\,sinh\left(\frac{\hbar\omega(k,\nu)}{2k_BT}\right)\right) \tag{14}$$

Under quasi harmonic approximation, the temperature dependency of C_V, F and S are shown in Fig. 7. The thermodynamic properties of $XTcO_3$ (X = K, Rb) are computed in temperature range changing from 0 to 1000 K, because it is known that quasi-harmonic Debye model is totally valid, if the temperature changes from 0 to 1000 K. We can see in Fig. 7 that at extremely low temperatures, C_V is proportional to T^3 following the famous Delong petit law, then after $T = 300\,K$, C_V increases rapidly with temperature and for higher temperatures, it converges to a constant. Helmholtz free energy F gradually decreases from positive to negative values that indicates the stability of our compounds However, S increases with raising temperature that suggests that increasing temperature causes a presence of more intense oscillations that influence the crystal plates.

4. Conclusions

The structural, electronic, elastic, mechanical, and thermodynamic properties of the cubic perovskite $XTcO_3$ (X = K, Rb) compounds were investigated from first-principles calculations. The computed elastic constants as well as phonon spectra, demonstrated that both compounds $XTcO_3$ (X = K, Rb) are found to be mechanically stable. In addition, both compounds exhibited brittle behavior with anisotropic character for

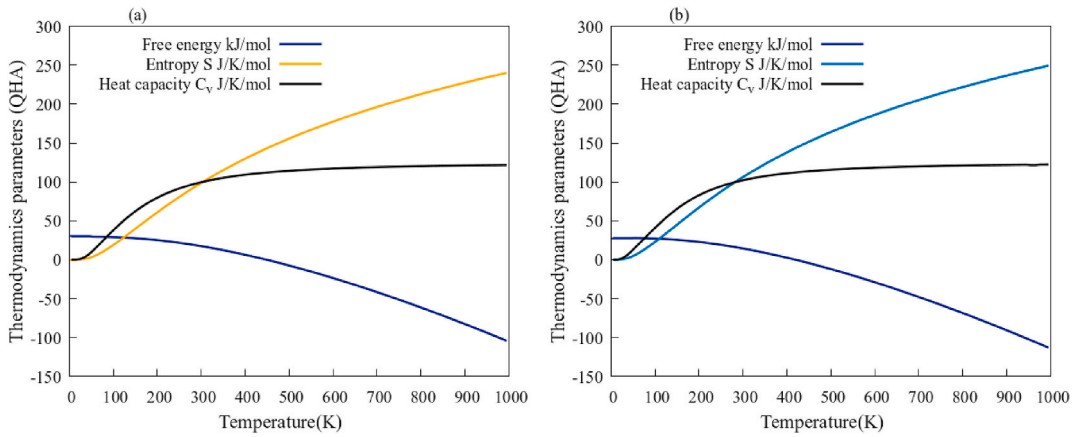

Fig. 7. Temperature dependence of heat capacity C_V, entropy S, Helmholtz-free energy F of (a)$KTcO_3$ and (b) $RbTcO_3$ compounds.

$KTcO_3$ and nearly isotropic character for $KTcO_3$. The examination of electronic properties reveals a metallic nature inherent in the analyzed compounds, substantiated by comprehensive assessments of both band structure and density of states. Finally, the thermodynamic properties including free energy, entropy, heat capacity and thermal expansion behavior were also computed using the quasi-harmonic approximation. Hence, our work has shown that XTcO3 (X = K, Rb) compounds can be used as innovative materials suitable for solid oxide fuel cells and linked functionalities.

CRediT authorship contribution statement

Toufik Nouri: Conceptualization. **Friha Khelfaoui:** Investigation. **Kadda Amara:** Methodology. **Abdelmadjid Bouhemadou:** Validation. **Fadila Belkharroubi:** Writing – original draft. **Y. Al-Douri:** Supervision, Writing – review & editing.

Declaration of competing interest

The authors declare that they have no known competing financial interests or personal relationships that could have appeared to influence the work reported in this paper.

Data availability

No data was used for the research described in the article.

References

[1] C.J. Rhodes, Perovskites and their potential use in solar energy applications, Sci. Prog. 97 (2014) 279–287.
[2] N. Erum, M.A. Iqbal, Mechanical and magneto-opto-electronic investigation of transition metal based fluoro-perovskites: an ab-initio DFT study, Solid State Commun. 264 (2017) 39–48.
[3] M.I. Hussain, R.A. Khalil, F. Hussain, M. Imran, A.M. Rana, S. Kim, Investigations of structural, electronic and optical properties of YInO3 (Y= Rb, Cs, Fr) perovskite oxides using mBJ approximation for optoelectronic applications: a first principles study, Mater. Sci. Semicond. Process. 113 (2020) 105064.
[4] M. Houari, B. Bouadjemi, S. Haid, M. Matougui, T. Lantri, Z. Aziz, S. Bentata, B. Bouhafs, Semiconductor behavior of halide perovskites AGeX 3 (A= K, Rb and Cs; X= F, Cl and Br): first-principles calculations, Indian J. Phys. 94 (2020) 455–467.
[5] W.-J. Yin, J.-H. Yang, J. Kang, Y. Yan, S.-H. Wei, Halide perovskite materials for solar cells: a theoretical review, J. Mater. Chem. A 3 (2015) 8926–8942.
[6] S.A. Dar, M.A. Ali, V. Srivastava, Investigation on bismuth-based oxide perovskites MBiO 3 (M= Rb, Cs, Tl) for structural, electronic, mechanical and thermal properties, Eur. Phys. J. B 93 (2020) 1–11.
[7] F. Moussa, M. Hennion, J. Rodriguez-Carvajal, H. Moudden, L. Pinsard, A. Revcolevschi, Spin waves in the antiferromagnet perovskite LaMn O 3: a neutron-scattering study, Phys. Rev. B 54 (1996) 15149.
[8] K.J. Choi, M. Biegalski, Y. Li, A. Sharan, J. Schubert, R. Uecker, P. Reiche, Y. Chen, X. Pan, V. Gopalan, Enhancement of ferroelectricity in strained BaTiO3 thin films, Science 306 (2004) 1005–1009.
[9] Z. Zhong, Y. Sugiyama, H. Ishiwara, Thickness dependences of polarization characteristics in Mn-substituted BiFeO3 films on pt electrodes, Jpn. J. Appl. Phys. 47 (2008) 6448.
[10] S. Sheoran, M. Kumar, P. Bhumla, S. Bhattacharya, Rashba spin splitting and anomalous spin textures in the bulk ferroelectric oxide perovskite KIO 3, Materials Advances 3 (2022) 4170–4178.
[11] W. Knafo, C. Meingast, A. Boris, P. Popovich, N. Kovaleva, P. Yordanov, A. Maljuk, R. Kremer, H.v. Löhneysen, B. Keimer, Ferromagnetism and lattice distortions in the perovskite YTiO 3, Phys. Rev. B 79 (2009) 054431.
[12] S. Zhang, F. Li, High performance ferroelectric relaxor-PbTiO3 single crystals: status and perspective, J. Appl. Phys. 111 (2012).
[13] G. Shirane, K. Suzuki, Crystal structure of Pb (Zr-Ti) O3, J. Phys. Soc. Jpn. 7 (1952), 333-333.
[14] J.C. Shaw, K.S. Liu, I.N. Lin, Modification of piezoelectric characteristics of the Pb (Mg, Nb) O3-PbZrO3-PbTiO3 ternary system by aliovalent additives, J. Am. Ceram. Soc. 78 (1995) 178–182.
[15] S.A. Dar, V. Srivastava, U.K. Sakalle, Ab initio high pressure and temperature investigation on cubic PbMoO 3 perovskite, J. Electron. Mater. 46 (2017) 6870–6877.
[16] M. Ren, X. Qian, Y. Chen, T. Wang, Y. Zhao, Potential lead toxicity and leakage issues on lead halide perovskite photovoltaics, J. Hazard Mater. 426 (2022) 127848.
[17] M. Lyu, J.H. Yun, P. Chen, M. Hao, L. Wang, Addressing toxicity of lead: progress and applications of low-toxic metal halide perovskites and their derivatives, Adv. Energy Mater. 7 (2017) 1602512.
[18] S. Yang, W. Fu, Z. Zhang, H. Chen, C.-Z. Li, Recent advances in perovskite solar cells: efficiency, stability and lead-free perovskite, J. Mater. Chem. A 5 (2017) 11462–11482.
[19] B. Yan, M. Jansen, C. Felser, A large-energy-gap oxide topological insulator based on the superconductor BaBiO3, Nat. Phys. 9 (2013) 709–711.
[20] S. Zhao, Z. Wei, S.A. Dar, Insight into the structural, electronic, elastic, mechanical, and thermodynamic properties of XReO3 (X= Rb, Cs, Tl) perovskite oxides: a DFT study, Z. Naturforsch. 74 (2019) 827–836.
[21] A. Dixit, D. Behera, S.K. Tripathi, A. Srivastava, R. Sharma, R. Khenata, H. Albalawi, Z. Mahmoud, S.K. Mukherjee, Vibrational, mechanical, electronic and thermodynamic properties of rhenium-based perovskites XReO3 (X= Li, Be) by an ab-initio computation, Mater. Sci. Eng., B 294 (2023) 116545.
[22] D. Behera, A. Dixit, K. Kumari, A. Srivastava, R. Sharma, S. Mukherjee, R. Khenata, A. Boumaza, S. Bin-Omran, Structural, elastic, mechanical, and thermodynamic characteristic of NaReO3 and KReO3 perovskite oxides from first principles study, The European Physical Journal Plus 137 (2022) 1345.
[23] P. Giannozzi, O. Andreussi, T. Brumme, O. Bunau, M.B. Nardelli, M. Calandra, R. Car, C. Cavazzoni, D. Ceresoli, M. Cococcioni, Advanced capabilities for materials modelling with Quantum ESPRESSO, J. Phys. Condens. Matter 29 (2017) 465901.
[24] P. Giannozzi, S. Baroni, N. Bonini, M. Calandra, R. Car, C. Cavazzoni, D. Ceresoli, G.L. Chiarotti, M. Cococcioni, I. Dabo, Quantum ESPRESSO: a modular and open-source software project for quantum simulations of materials, J. Phys. Condens. Matter 21 (2009) 395502.
[25] N.T. Hung, A.R. Nugraha, R. Saito, Quantum ESPRESSO Course for Solid-State Physics, CRC Press, 2022.
[26] D.J. Singh, L. Nordstrom, Planewaves, Pseudopotentials, and the LAPW Method, Springer Science & Business Media, 2006.
[27] J.P. Perdew, K. Burke, M. Ernzerhof, Generalized gradient approximation made simple, Phys. Rev. Lett. 77 (1996) 3865.
[28] M. Ernzerhof, G.E. Scuseria, Assessment of the perdew–burke–ernzerhof exchange-correlation functional, J. Chem. Phys. 110 (1999) 5029–5036.
[29] G. Kresse, D. Joubert, From ultrasoft pseudopotentials to the projector augmented-wave method, Phys. Rev. B 59 (1999) 1758.
[30] A. Dal Corso, Elastic constants of beryllium: a first-principles investigation, J. Phys. Condens. Matter 28 (2016) 075401.

[31] T. Tohei, H.-S. Lee, Y. Ikuhara, First principles calculation of thermal expansion of carbon and boron nitrides based on quasi-harmonic approximation, Mater. Trans. 56 (2015) 1452–1456.
[32] V. Tyuterev, N. Vast, Murnaghan's equation of state for the electronic ground state energy, Comput. Mater. Sci. 38 (2006) 350–353.
[33] H. Hamada, K. Boudia, F. Khelfaoui, K. Amara, T. Nouri, O. Sadouki, Ferrimagnetic half-metallicity of the new quaternary heusler alloy CoCrScIn: FP-lapw method, in: Spin, World Scientific, 2021 2150017.
[34] M. Rizwan, A. Afaq, A. Aneeza, Lattice dynamics of Ru2FeX (X= Si, Ge) full heusler alloys, Phys. B Condens. Matter 537 (2018) 225–227.
[35] M. Born, K. Huang, Dynamical Theory of Crystal Lattices, Oxford university press, 1996.
[36] F. Mouhat, F.-X. Coudert, Necessary and sufficient elastic stability conditions in various crystal systems, Phys. Rev. B 90 (2014) 224104.
[37] E. Schreiber, O.L. Anderson, N. Soga, J.F. Bell, Elastic Constants and Their Measurement, 1975.
[38] S. Pugh, XCII. Relations between the elastic moduli and the plastic properties of polycrystalline pure metals, London, Edinburgh Dublin Phil. Mag. J. Sci. 45 (1954) 823–843.
[39] Y. Rakita, S.R. Cohen, N.K. Kedem, G. Hodes, D. Cahen, Mechanical properties of APbX3 (A= Cs or CH3NH3; X= I or Br) perovskite single crystals, MRS Communications 5 (2015) 623–629.
[40] R. Wentzcovitch, B. Karki, S. Karato, C. Da Silva, High pressure elastic anisotropy of MgSiO3 perovskite and geophysical implications, Earth Planet Sci. Lett. 164 (1998) 371–378.
[41] H.-C. Cheng, C.-F. Yu, W.-H. Chen, First-principles density functional calculation of mechanical, thermodynamic and electronic properties of CuIn and Cu2In crystals, J. Alloys Compd. 546 (2013) 286–295.
[42] T. Nouri, F. Khelfaoui, Y. Benallou, H. Lakhdari, K. Amara, H. Boutaleb, M. Dahmani, Theoretical design of novel half-metallic alloys XMg 3 O 4 (X= Li, Na, K, Rb), Appl. Phys. A 127 (2021) 1–9.
[43] B. Huang, Y.-H. Duan, W.-C. Hu, Y. Sun, S. Chen, Structural, anisotropic elastic and thermal properties of MB (M= Ti, Zr and Hf) monoborides, Ceram. Int. 41 (2015) 6831–6843.
[44] Q. Wu, S. Li, Alloying element additions to Ni3Al: site preferences and effects on elastic properties from first-principles calculations, Comput. Mater. Sci. 53 (2012) 436–443.
[45] V. Kanchana, G. Vaitheeswaran, Y. Ma, Y. Xie, A. Svane, O. Eriksson, Density functional study of elastic and vibrational properties of the Heusler-type alloys Fe 2 VAl and Fe 2 VGa, Phys. Rev. B 80 (2009) 125108.